

CENTRAL ASIAN JOURNAL OF THEORETICAL AND APPLIED SCIENCE

https://cajotas.casjournal.org/index.php/cajotas

Volume: 08 Issue: 01 | January 2027 ISSN: 2660-5317

Article

Synthesis, Characterization, Biological Activity and Nano-Structure Study of Isoxazole-Dithiocarbamate Complexes

Tohama B. Abdullah[1]

1. Department of Chemistry, College of Science, Tikrit Unversity, Tikrit, Iraq

* Correspondence: Tuhama.baban@tu.edu.iq

Abstract: A new series of transition metal dithiocarbamate complexes derived from 3-amino-5-methylisoxazole, [ML2] [M = Fe(II) (1), Ni(II) (2), Cu(II) (3), Pt(II) (4), Cd(II) (5), Hg(II) (6)] and [PhHgL]2 (7), were synthesized by one-pot reaction of the isoxazole amine with CS2 in the presence of KOH followed by treatment with the corresponding metal salts. The ligand scaffold incorporates the coordination versatility of the dithiocarbamate moiety and the established bioactive profile of the isoxazole pharmacophore. Characterization of the complexes was done by molar conductivity, FT-IR, 1H and 13C NMR spectroscopy, powder XRD, SEM and EDX analysis. The IR spectra confirmed the bidentate κ²-S,S′ coordination of the dithiocarbamate moiety via the characteristic ν(C=S), ν(C–S), ν(C–N) and ν(C=N) bands, while NMR data supported the proposed structures with the CSS carbon appearing at δ 200.26–203.76 ppm. XRD analysis showed that the Fe and Pt complexes are mostly amorphous with short-range order, while the Cd and Ni complexes are semi-crystalline with nanoscale ordered domains of about 2.6–2.8 nm as estimated from the Debye–Scherrer equation. SEM images showed different morphologies which vary from plate-like, fibrous, granular, agglomerated and cauliflower-like microstructures. The particle size was in the nanometer range. EDX analysis confirmed the presence of the expected metal, sulfur, oxygen and carbon in all complexes. The antibacterial activity of complexes 1–4 against Staphylococcus aureus (Gram-positive) and Escherichia coli (Gram-negative) was investigated by the agar diffusion method. All the complexes show moderate activity, where the platinum complex [PtL_2] has the highest activity (16 mm against S. aureus and 19 mm against E. coli) and the nickel complex [NiL_2] has the lowest activity, although none of them reach the level of the standard antibiotic tetracycline (23 and 26 mm, respectively).

Keywords: Dithiocarbamate; Isoxazole; Metal complexes; Nanostructure; Antibacterial activity; XRD; SEM

Citation: Abdullah, T. B. Synthesis, Characterization, Biological Activity and Nano-Structure Study of Isoxazole-Dithiocarbamate Complexes. Central Asian Journal of Theoretical and Applied Science 2027, 8(1), 26-42

Received: 13th Aug 2026
Revised: 28th Sep 2026
Accepted: 15th Oct 2026
Published: 08th Nov 2026

Copyright: © 2027 by the authors. Submitted for open access publication under the terms and conditions of the Creative Commons Attribution (CC BY) license (https://creativecommons.org/licenses/by/4.0/)

1. Introduction

Dithiocarbamate ligands ($R_2NCS_2^-$) are privileged in coordination chemistry because of their remarkable versatility as soft sulfur-donating chelators[**1-8**]. Their ability to stabilize metal centers in a wide range of oxidation states, and the ease with which the structure can be modified by varying the amine backbone, has maintained interest in their metal complexes for applications ranging from medicinal chemistry to materials science and catalysis[**1-8**]. The dithiocarbamate moiety coordinates typically in a bidentate κ²-S,S′ fashion, resulting in the formation of four-membered chelate rings with a small bite angle, which has a profound effect on the geometry and electronic properties of the resulting complexes . The structural rigidity and stability of these systems are also attributed to the partial double bond character of the C–N and C–S bonds in the thioureide framework,

while substituents on the nitrogen atom modulate supramolecular aggregation through secondary M···S of the interactions[**1-8**].

Dithiocarbamate complexes have the advantage of being synthetically accessible[**1-8**]. The one-pot reaction of a primary or secondary amine with carbon disulfide under basic conditions produces the dithiocarbamate salt in situ, which on treatment with a metal halide yields the corresponding complex, often in high yield and with straightforward purification[**3,4**]. The modular nature of the approach allows the incorporation of a variety of functional groups, alkyl, aryl and heterocyclic substituents, into the ligand framework, which allows for the systematic tuning of steric and electronic properties[**3,4,9,10**]. The ligand precursor of the present work is prepared from 3-amino-5-methylisoxazole, a heterocyclic amine that introduces an isoxazole pharmacophore into the dithiocarbamate backbone[**11**]. Isoxazole and its derivatives are well known in medicinal chemistry for their broad spectrum of biological activities including anti-inflammatory, antimicrobial, anticancer and analgesic properties and have been used as key structural motifs in several marketed drugs [**12-15**]. Thus, the introduction of an isoxazole moiety into a dithiocarbamate ligand backbone represents a rational design strategy for merging the coordination variability of the dithiocarbamate group with the established bioactivity profile of the isoxazole ring.

Metal dithiocarbamate complexes are extensively studied for their biological potential, industrial applications, and catalytic applications. In particular, Cu(II), Pt(II), Pd(II), Mn(II) and Zn(II) dithiocarbamates have exhibited promising anticancer activity, usually through mechanisms involving proteasome inhibition, DNA interaction and induction of apoptosis [**1-8**]. This dual utility, as bioactive agents and as molecular precursors to functional materials, emphasizes the importance of systematic structural and spectroscopic characterization of new dithiocarbamate derivatives[**1-8,16-34**].

In the present study, a series of transition metal complexes (**1**–**6**) and a phenylmercury(II) derivative (**7**) with the 3-amino-5-methylisoxazole derived dithiocarbamate ligand (LH) have been synthesized. The metal centers selected allow to investigate how the dithiocarbamate ligand accommodates different coordination geometries and oxidation state preferences. The following sections describe the synthesis, spectroscopic characterization and structural features of the complexes (**1**–**7**) and are intended to contribute to a more general understanding of isoxazole-functionalized dithiocarbamate coordination chemistry.

2. Materials and Methods

Experimental part

2.1 Materials and Physical Measurements

The infrared spectra of the prepared compounds were measured by using a SHIMADZU-FTIR-8400S spectrophotometer instrument in the range of 400–4000 cm^{-1}, using KBr pellets. The proton nuclear magnetic resonance (^{1}H-NMR) spectra were measured using a Varian Unity Spectrometer (300 MHz), with DMSO-d_6 as the solvent, at the Central Laboratory, University of Tehran. Scanning electron microscopy (SEM) images of the prepared complexes were recorded using a JEOL JSM-6390 LVSEM scanning electron microscope at an accelerating voltage of 15–20 kV and at different magnifications. Powder X-ray diffraction (XRD) patterns were recorded using a Bruker D8 Advanced instrument with Cu Kα radiation (λ = 1.5405 Å) at the Central Laboratory, College of Science, University of Tehran, Iran. All materials used in this study were purchased from Merck or Alfa Aesar and were used without any further purification.

2.2. General procedure for the preparation of 3-amino-5-methyl isoxazole dithiocarbamate Complexes (1–7)

The complexes (**1–7**) were prepared using one pot method according to the following general procedure: In round-bottom flask (100mL) on the ice bath (0-5°C), a solution of potassium hydroxide (0.05 g, 0.89 mmol) in ethanol (10 mL) was added to a solution of 3-amino-5-methyl isoxazole (0.1 g, 0.5 mmol) in ethanol (10 mL), then an excess of CS_2 (0.5 mL) was added to afford a light-yellow solution, then the mixture was stirred for one

hour. An aqueous solution of the inorganic salt ions {$FeCl_2·4H_2O$, $NiCl_2·6H_2O$, $CuCl_2·2H_2O$, K_2PtCl_4, $CdCl_2$, $HgCl_2$, and PhHg(oAc)} (0.005 mol) in (10 mL) was then added to the freshly ligand solution prepared. A gradual color change was observed upon addition. The mixture was stirred for one hour again, after which the resulting precipitates were filtered, washed with distilled water and ethanol, collected, and then dried under vacuum to give a dark brown powder for [FeL_2] (**1**) (Yield: 0.053 g,53%, m. p: 160–162°C), dark brown powder for [NiL_2] (**2**) (Yield: 0.071 g,71%, m. p: 211–213°C), dark yellow powder for [CuL_2] (**3**) (Yield: 0.04 g,67%, m. p: 168–170°C), dark brown powder for [PtL_2] (**4**) (Yield: 0.1 g, 50%, m. p: 180–183°C), Pale yellow powder for [CdL_2] (**5**) (Yield: 0.89 g, 75%, m. p: 161–164°C), White powder for [HgL_2] (**6**) (Yield: 0.76 g, 78%, m. p: 210-212°C), White powder for [$PhHgL]_2$ (**7**) (Yield: 0.69 g, 69%, m. p: 129-131°C),

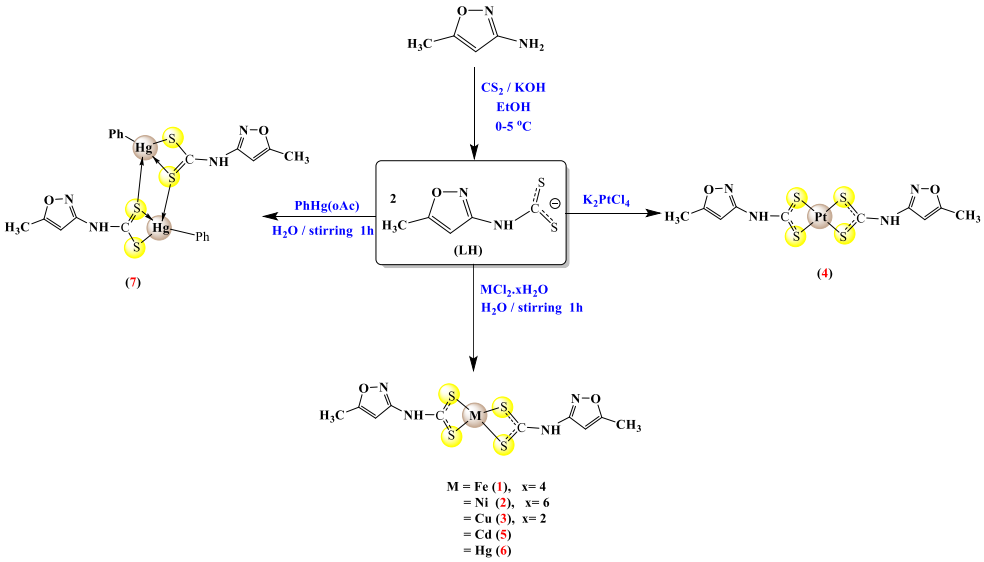
2.3 Antibacterial study

The antibacterial effectiveness of the newly designed complexes was evaluated using the agar diffusion method against four harmful bacteria: *Staphylococcus aureus, and Escherichia coli*. the chemical solution prepared in DMSO (10^{-3} M) was allocated into the wells of each plate. The measurements of the inhibitory zone were evaluated at 37 ˚C after a 24-hour incubation. The tetracycline antibiotic solution served as the positive control in this research.

3. Results

3.1. Synthesis

The complexes of the type [ML_2] { M = Fe(**1**), Ni(**2**), Cu(**3**), Pt(**4**), Cd(**5**), and Hg(**6**)} and [$PhHgL]_2$ (**7**) were prepared by a one-pot method, in the first step the freshly ligand solution was prepared by treated equivalent molar ratio of 3-amino-5-methyl isoxazole and carbon disulfide (CS_2) in present KOH as a base, then the mixture was added to a solution of one of the metal salts, at a ligand-to-metal ratio of (1:2) in ethanol (**Scheme 1**). All of the above complexes were characterized by molar conductivity, infrared (IR) and proton nuclear magnetic resonance (^{1}H-NMR) spectroscopic techniques, in addition to studying some of their nanoscale properties.



Scheme 1: synthetic pathway of the prepared complexes (**1-7**)

3.2. IR Data of the [ML_2] { M = Fe(1), Ni(2), Cu(3), Pt(4), Cd(5), and Hg(6)} and [$PhHgL]_2$ (7)

The infrared spectra of the complexes with the formula [ML_2] showed two bands attributable to the CSS group, one within the range of 1008–1031 cm^{-1} and the other within the range of 850–999 cm^{-1}, which were assigned to ν(C=S) and ν(C–S), respectively. A band within the range of 1215–1290 cm^{-1} was assigned to the stretching vibration of the ν(C–N) group. The spectra also showed a medium-intensity band within the range of 1435–1479 cm^{-1}, attributed to the stretching vibration of the ν(C=N) group. In addition, a weak-to-

medium intensity band within the range of 2926–2983 cm^{-1} was attributed to the stretching vibration of the aliphatic ν(C–H) group. The spectra also exhibited a weak-to-medium intensity band within the range of 3009–3142 cm^{-1}, attributed to the stretching vibration of the aromatic ν(C–H) group. Furthermore, a weak-to-medium intensity band within the range of 3135–3423 cm^{-1} was attributed to the stretching vibration of the ν(N–H) group. The remaining bands are listed in **Table 1**

Table 1. Infrared absorption values (cm^{-1}) for the prepared complexes.

Seq	Complexes	υ(N-H)	υ(C-H)		υ(C=C)	υ(C=N)	υ (C-N)	υ(C=S)	υ(C-S)
			Ar.	Alp.					
1	[FeL_2]	3417m	3025w	2982w	1620w	1442w	1251s	1028s	850w
2	[NiL_2]	3402w	3009w	2983w	1710w	1435w	1250s	1026s	999m
3	[CuL_2]	3344m	3142w	2978w	1635s	1479m	1288m	1018w	939w
4	[PtL_2]	3319m	3140w	2926w	1635s	1479m	1284m	1008w	947w
5	[CdL_2]	3362w	3037w	2974m	1631w	1437m	1290w	1031s	860w
6	[HgL_2]	3423w	3142w	2982w	1587s	1471w	1255w	1008w	864w
7	[$PhHgL]_2$	3135w	3055m	2982m	1573w	1471w	1215s	1024s	854w

3.3 NMR Data of the [ML_2] { M = Pt(4), Cd(5), and Hg(6)} and [$PhHgL]_2$ (7)

The ^{1}H NMR spectra of the complexes with the formula [ML_2] (**4**-**6**) (**Figure 1**) (**Table 2**) showed three singlet peaks. The first peak showed at δH = (12.34 – 12.63) ppm, due to the proton of NH group. The second peak displayed at δH = (6.49 – 6.62) ppm, due to the proton of CH group of the oxazole ring. The third peak at δH = (3.73 – 3.83) ppm, due to the protons of methyl group. The ^{1}H NMR spectrum of the complex [$PhHgL]_2$ (**Figure 2**) displayed a multiplate peak at δH = 7.37 (m, 10H) ppm, due to the protons of phenyl ring, in addition three singlet peaks at δH = 12.58 ppm (s, 2H, NH), δH = 6.58 ppm (s, 2H, CH), δH = 3.38 ppm (s, 6H, CH_3). These results supported by the ^{13}C NMR spectra (**Figure 3-5**). The chemical shift of the carbon atom of the CSS group displayed at the δC = (200.26 – 203.76) ppm, whereas the δC of the CH of oxazole ring displayed at (95.99 – 98.55) ppm, Also, the δC of the O-**C**=C of oxazole ring displayed at (167.73 – 169.89) ppm. Another chemical shift is listed in the **Table 2**.

Table 2. Chemical shift in the NMR spectra (^{1}H and ^{13}C in ppm)

^{1}H NMR data (δ, ppm)

Seq.	Complexes	NH	CH	CH_3	Other
1	[PtL_2]	**12.63 (s,2H)**	**6.62 (s,2H)**	**3.73 (s,6H)**	**-**
2	[CdL_2]	**12.47 (s,2H)**	**6.49 (s,2H)**	**3.81 (s,6H)**	**-**
3	[HgL_2]	**12.34 (s,2H)**	**6.58 (s,2H)**	**3.83 (s,6H)**	**-**
4	[$PhHgL]_2$	**12.58 (s,2H)**	**6.58 (s,2H)**	**3.83 (s,6H)**	**7.37(m, 10H)**

^{13}C NMR data (δ, ppm)

Seq.	Complexes	**CSS**	**O-C=C**	**C=N**	**=C-H**	**CH_3**	Other
1	[PtL_2]	**200.26**	**168.88**	**156.76**	**95.99**	**14.61**	**-**
2	[CdL_2]	**203.76**	**169.89**	**158.64**	**98.45**	**12.77**	**-**
3	[HgL_2]	**201.67**	**167.73**	**157.91**	**97.83**	**13.91**	**-**
4	[$PhHgL]_2$	**202.34**	**168.09**	**156.87**	**98.55**	**14.31**	**137.53, 130.09,**

^{1}H NMR data (δ, ppm)					
Seq.	Complexes	NH	CH	CH_3	Other
					128.86, 128.41

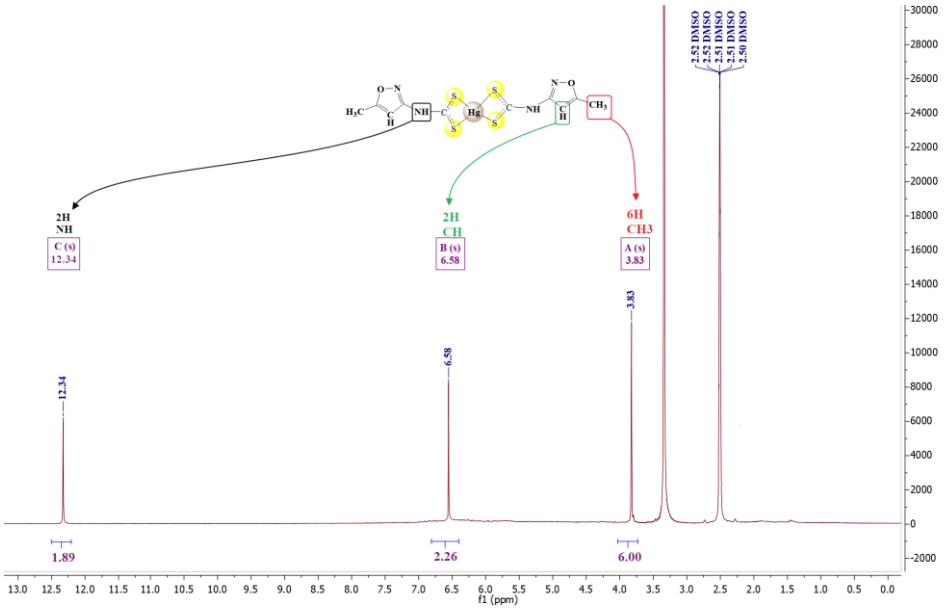


Figure 1: ^{1}H NMR spectrum of the complex $[HgL_2]$

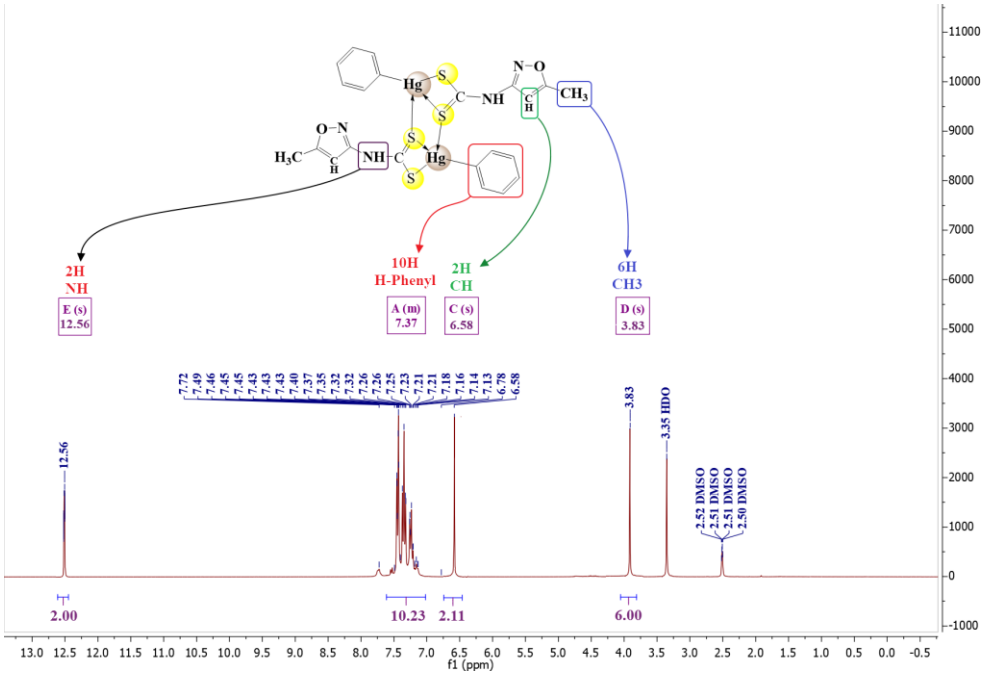


Figure 2: ^{1}H NMR spectrum of the complex $[PhHgL]_2$

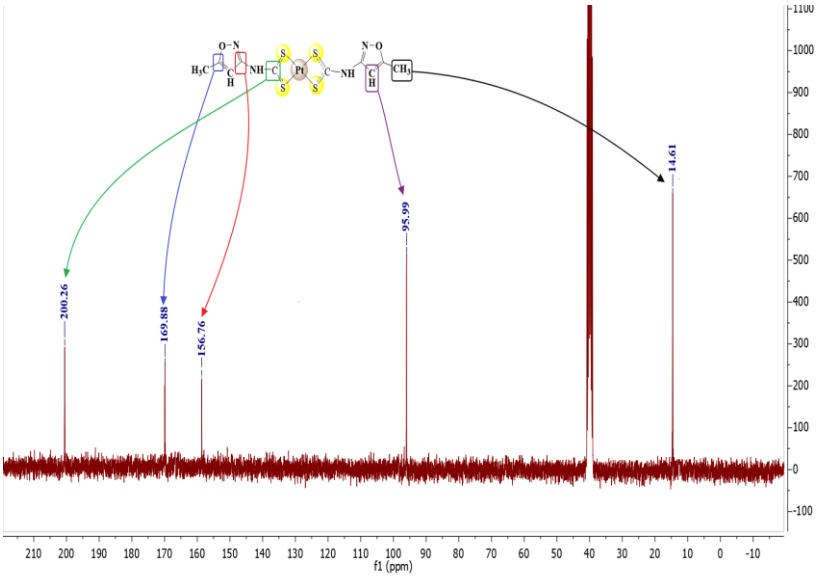


Figure 3: ^{13}C NMR spectrum of the complex $[PtL_2]$

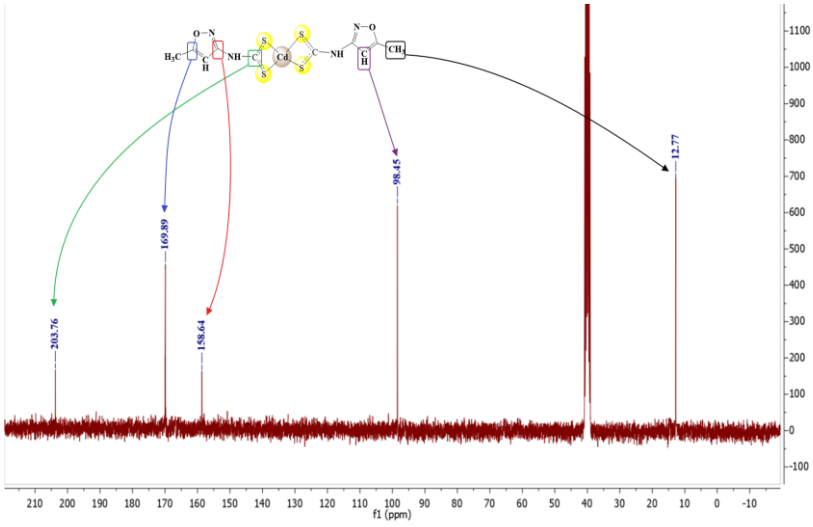


Figure 4: ^{13}C NMR spectrum of the complex $[CdL_2]$

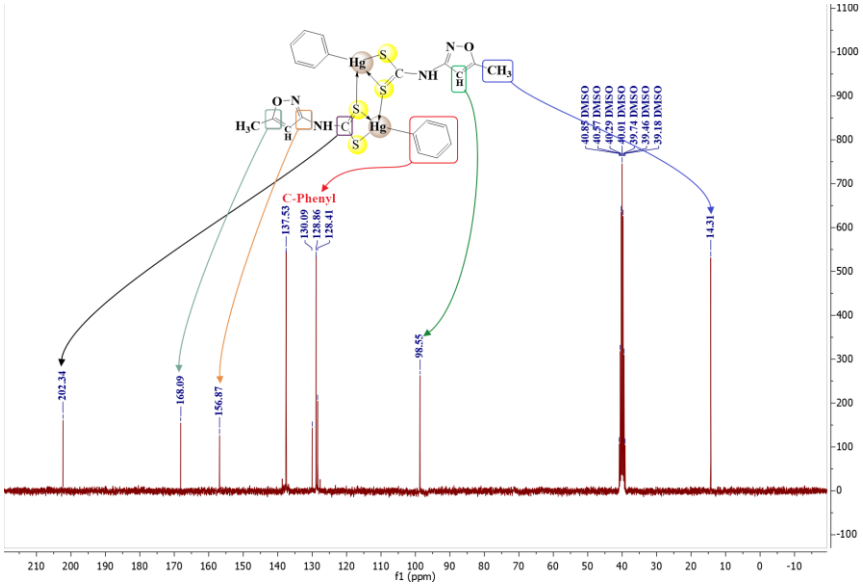


Figure 5: ^{13}C NMR spectrum of the complex $[PhHgL]_2$

3.3. Powder XRD analysis

Powder X-ray diffraction (XRD) (**Figure 6**) was employed to investigate the crystalline nature and crystallite size of the prepared metal complexes. The diffraction patterns exhibited a number of sharp, high-intensity peaks, confirming the crystalline nature of the complexes. The diffraction peaks were analyzed on the basis of Bragg's law, and the corresponding Miller indices (hkl) were assigned. In addition, the crystallite sizes were estimated using the Debye–Scherrer equation, based on the full width at half maximum (FWHM) values of the diffraction peaks. The results showed that the crystallite sizes fall within the nanometer range, confirming the formation of nanocrystalline structures.

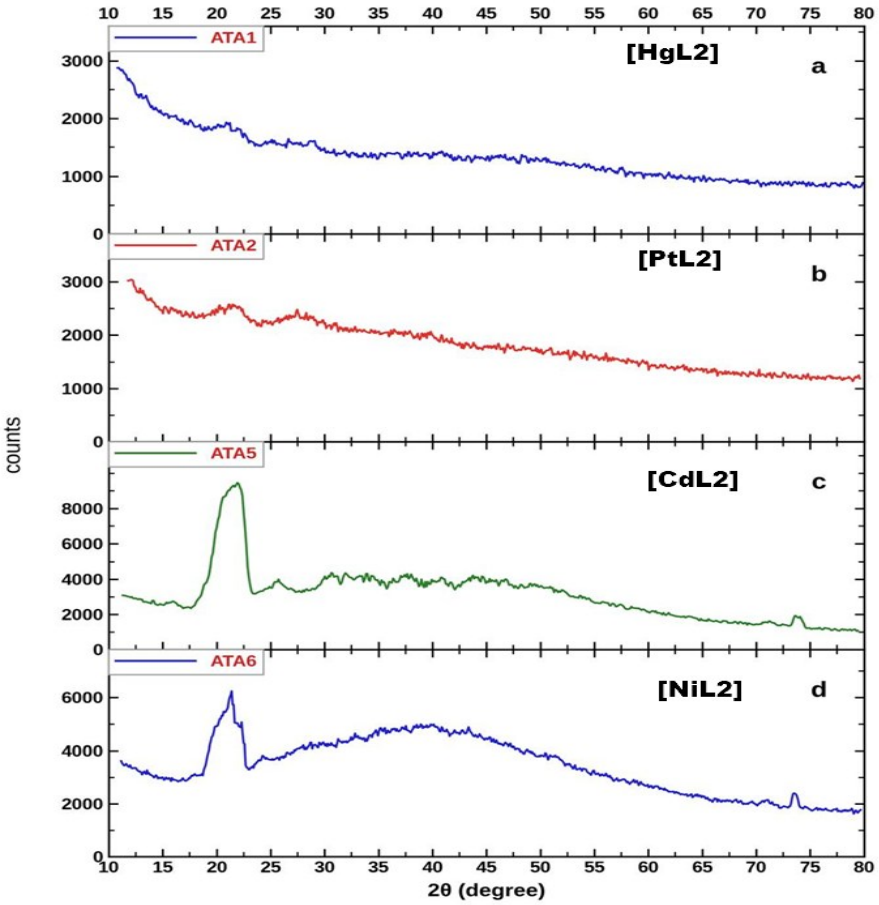


Figure 6: XRD patten of the prepared complexes

Powder X-ray diffraction (XRD) analysis of the platinum and iron complexes, [PtL_2] and [FeL_2], showed a very low degree of crystallinity. The background decreases from approximately 3000 counts at low angles to approximately 1000 counts at 80°, and is superimposed by two weak humps at 2θ ≈ 21°–21.5° and ≈ 27.5°–28.5°, which correspond to approximate interplanar spacings of ≈ 4.1–4.2 Å and ≈ 3.1–3.2 Å, respectively, according to Bragg's equation ($n\lambda = 2d \sin\theta$). The intensity of these two humps does not exceed a few hundred counts above the baseline, indicating that the proportion of the ordered phase in these two samples is negligible and that the predominant structure is amorphous with short-range order. The positions of the two humps in the two samples are close to each other, which suggests similar mean interplanar spacings in the two samples, with a slight difference in the degree of ordering.

As for the cadmium and nickel complexes, [CdL_2] and [NiL_2] , a distinct principal peak appears at 2θ ≈ 21.5°–22.0° (d ≈ 4.0–4.1 Å). In sample [CdL_2] which belongs to the cadmium complex, the peak intensity reached approximately 9400 counts (i.e., approximately 6400 net counts above the baseline), with a full width at half maximum (FWHM) of approximately 3.1°; a weak peak also appeared at ≈ 25.7° (d ≈ 3.46 Å), together

with two shoulders near ≈ 20.2° and ≈ 22.4°, which suggests the overlap of more than one component within this peak. In sample ATA6, which belongs to the nickel complex, the peak lies at approximately the same position but with a lower intensity (approximately 6100 counts, i.e., ≈ 2800 net counts) and a width of approximately 2.9°.

A broad halo extending between ≈ 28° and ≈ 55° is superimposed on these two peaks; in ATA5 it exhibits two closely spaced maxima (≈ 32° and ≈ 44°), whereas in ATA6 it is centered more regularly around ≈ 39° (d ≈ 2.3 Å). The coexistence of a relatively intense peak and a broad halo in the same pattern indicates a semi-crystalline structure, in which nanosized ordered domains coexist with an amorphous phase. The large peak width indicates that these ordered domains are very small and/or highly defective.

By applying the Scherrer equation, $D = K\lambda / (\beta \cos\theta)$, with K = 0.9, the dimensions of the ordered domains are estimated at approximately 2.6 nm for sample ATA5 and approximately 2.8 nm for sample [NiL_2]. It should be noted that these values are approximate and represent a lower limit of the coherence length, because the measured width includes contributions from instrumental broadening and from the superimposed amorphous phase, and no correction was applied for either.

3.4 SEM image

The SEM images of seven synthesized metal complexes (**1–7**) shown in **Figure 7**. The SEM image of the [FeL_2] complex (**Figure 7 A**) exhibit the particles a layered, plate-like, and somewhat fibrous morphology, large, smooth-surfaced flakes are visible, with measured dimensions ranging from ~67 nm to ~874 nm. and the surface appears relatively dense and compact, with some stacked lamellar structures. and the particle edges are irregular, and some rod-like/fibrous fragments are present (e.g., 110.4 nm, 244.4 nm). Whereas the SEM image of the [NiL_2] (**2**) and [CuL_2] (**3**) (**Figure 7B and 7C**) shown the morphology is highly agglomerated and granular, with irregular, blocky, and flaky particles, and the sizes range from ~40 nm to ~900 nm. The surface is rough and porous, with many smaller nanoparticles adhering to larger aggregates. Also, the figure distinct angular and jagged edges are visible, suggesting brittle fracture or crystalline aggregation. The SEM image of the [PtL_2] complex (**4**) (**Figure 7D**) displayed the morphology is a fused irregular and the sizes range from ~40 nm to ~625 nm.

The SEM image of the [CdL_2] complex exhibit the particles as elongated, rod-like or fibrous structures with rough surfaces, alongside smaller particles. The complex exhibits a fibrous or rod-like morphology with diameters in the 30–80 nm range and lengths up to ~600 nm. This suggests anisotropic growth, possibly due to the ligand's coordination geometry. [HgL_2] complex a high-magnification SEM image of the (**6**). The image reveals a highly agglomerated, porous, and coral-like or cauliflower-like microstructure. The material consists of numerous small, roughly spherical primary particles that have clustered together into larger, irregular secondary aggregates. The surface appears rough and granular, with visible voids and interparticle spaces throughout the structure. The [$PhHgL]_2$ complex (**7**) forms a bimodal nanostructure consisting of a large, smooth, plate-like substrate (≥1–2 μm) decorated with smaller, irregular particles (43–137 nm) and some larger angular fragments (420–802 nm). The elemental composition of the prepared complexes, as determined by energy dispersive X-ray analysis (EDX), is shown in **Figure 8**. It was confirmed that Fe, Ni, Co, Cu, Pt Cd and Hg, and O were present in the complexes.

Table 2. Energy dispersive X-ray analysis (EDX) of the prepared complex

	Map Sum Spectrum				
	Element	**Line Type**	**Weight %**	**Weight % Sigma**	**Atomic %**
[FeL_2]	**C**	**K series**	**17.86**	**0.45**	**30.18**
	O	**K series**	**42.23**	**0.36**	**53.58**
	S	**K series**	**6.43**	**0.11**	**4.07**
	Fe	**K series**	**33.48**	**0.33**	**12.17**
	Total		**100**		**100**

	Element	Line Type	Weight %	Weight % Sigma	Atomic %
	C	K series	29.65	0.76	49.64
[NiL_2]	O	K series	22.83	0.38	23.69
	S	K series	19.44	0.29	17.05
	Ni	K series	28.08	0.43	9.62
	Total		100		100
	Element	Line Type	Weight %	Weight % Sigma	Atomic %
	C	K series	42.59	0.47	44.61
[CuL_2]	O	K series	17.68	0.33	16.67
	S	K series	25.89	0.43	24.38
	Cu	L series	13.84	0.25	14.34
	Total		100		100
	Element	Line Type	Weight %	Weight % Sigma	Atomic %
	C	K series	39.32	0.54	39.63
[PtL_2]	Pt	M series	31.62	0.46	29.86
	O	K series	12.61	0.31	14.74
	S	K series	16.45	0.12	15.77
	Total		100		100
	Element	Line Type	Weight %	Weight % Sigma	Atomic %
	O	K series	11.18	0.38	19.01
[CdL_2]	S	K series	21.54	0.29	18.33
	Cd	L series	38.93	0.53	19.45
	C	K series	28.35	0.67	43.21
	Total		100		100
	Element	Line Type	Weight %	Weight % Sigma	Atomic %
	C	K series	48.5	0.47	83.01
[HgL_2]	S	K series	8.45	0.16	5.42
	O	K series	6.05	0.27	7.78
	Hg	M series	37	0.43	3.79
	Total		100		100
	Element	Line Type	Weight %	Weight % Sigma	Atomic %
	C	K series	30.36	0.6	44.12
[$PhHgL]_2$	S	K series	11.88	0.18	18.75
	Hg	M series	47.12	0.54	22.37
	O	K series	10.64	0.3	14.76
	Total		100		100

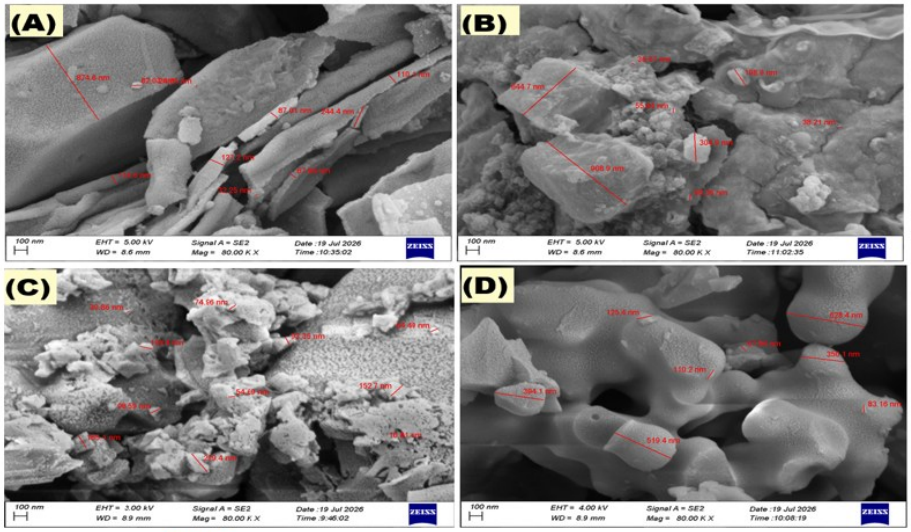


Figure 7: SEM image of the complexes (A) [FeL_2], (B) [CoL_2], (C) [CuL_2], (D) [PtL_2]

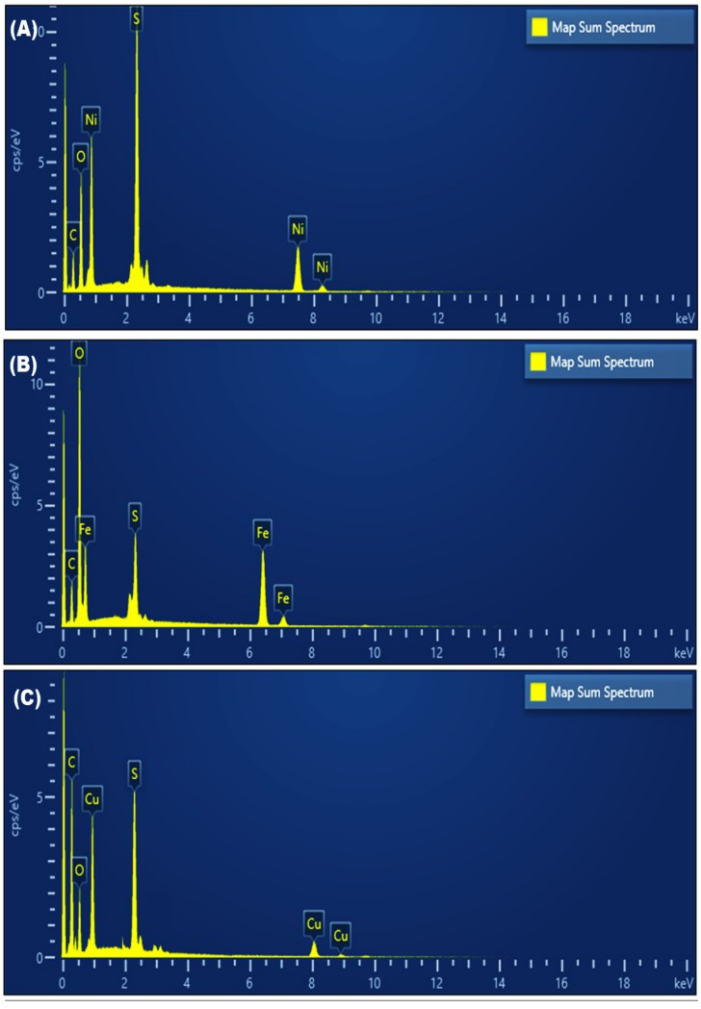


Figure 8: EDX spectra of the complexes (A) [NiL_2], (B) [FeL_2], (C) [CuL_2]

3.5 Biological activity

The biological activity of the prepared complexes (**1–4**) (**Table 3** and **Figure 9**) was evaluated against two bacterial strains: *Staphylococcus aureus* (Gram-positive) and *Escherichia coli* (Gram-negative). The activity was measured as the Diameter of Inhibition Zone (DIZ) in millimeters, with Tetracycline used as a standard reference antibiotic. comparison with standard antibiotic (Tetracycline)

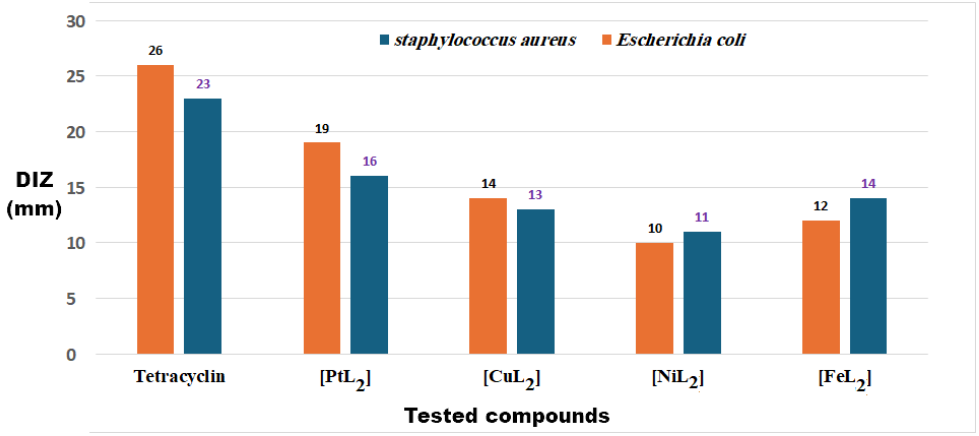


Figure 3: Histogram of the biological activity of the of preapred complexes

Table 9: Diameter inhibition zone (mm) of the prepared complexes

Complexes	*staphylococcus aureus*	*Escherichia coli*
[FeL_2]	14	12
[NiL_2]	11	10
[CuL_2]	13	14
[PtL_2]	16	19
Tetracycline	23	26

All prepared complexes showed lower activity than Tetracycline against both bacterial strains, indicating that while they possess antimicrobial properties, they are less potent than the standard drug. The order of activity against *Staphylococcus aureus* (Gram-positive) was:

Tetracycline > [PtL_2] > [FeL_2] > [CuL_2] > [NiL_2]

while the order of activity against *Escherichia coli* (Gram-negative) was:

Tetracycline > [PtL_2] > [CuL_2] > [FeL_2] > [NiL_2]

Platinum complex [PtL_2] is the most active among all prepared complexes against both bacterial strains, with DIZ values of 16 mm (*S. aureus*) and 19 mm (*E. coli*). This suggests that the platinum center plays a significant role in enhancing antimicrobial activity. Nickel complex [NiL_2] is the least active against both strains (11 mm for *S. aureus* and 10 mm for *E. coli*). Gram-negative *E. coli* is generally more susceptible to the complexes than Gram-positive *S. aureus*, except for [FeL_2], which showed slightly higher activity against *S. aureus* (14 mm) than *E. coli* (12 mm). Copper complex [CuL_2] showed moderate activity, with slightly better effect on *E. coli* (14 mm) than *S. aureus* (13 mm). Iron complex [FeL_2] exhibited comparable activity against both strains (14 mm for *S. aureus*, 12 mm for *E. coli*).

4. Discussion

The findings of this study demonstrate that the successful synthesis of isoxazole-derived dithiocarbamate metal complexes is accompanied by distinct spectroscopic, structural, morphological, and antibacterial characteristics. The preparation of seven complexes containing Fe(II), Ni(II), Cu(II), Pt(II), Cd(II), Hg(II), and phenylmercury(II) through a one-pot synthesis approach highlights the versatility of the dithiocarbamate ligand in coordinating with different metal centers. The observed variations in physical properties suggest that the identity of the coordinated metal influences the structural organization and physicochemical behavior of the resulting compounds. These observations are consistent with the coordination chemistry principles discussed by Hogarth [3], who emphasized the structural diversity and coordination flexibility of metal

dithiocarbamate complexes. Furthermore, the findings support the broader applications of dithiocarbamate compounds described by Ajiboye et al. [8], particularly their potential as functional materials and biologically active coordination compounds. The incorporation of the isoxazole moiety provides an additional heterocyclic structural component that may contribute to the electronic characteristics of the ligand framework. Therefore, the synthesized compounds represent a useful series for investigating the relationship between metal coordination, nanoscale structural organization, and antibacterial performance.

The Fourier-transform infrared spectroscopy results provide evidence supporting the proposed coordination behavior of the dithiocarbamate ligand. The appearance of characteristic absorption bands at 1008–1031 cm^{-1} and 850–999 cm^{-1}, assigned to C=S and C–S stretching vibrations, respectively, indicates the presence of the dithiocarbamate functional group in the prepared complexes. Additionally, the C–N stretching bands observed at 1215–1290 cm^{-1} and the C=N absorption bands at 1435–1479 cm^{-1} support the retention of the ligand framework following metal complexation. These spectroscopic characteristics are compatible with the proposed bidentate κ^2-S,S′ coordination mode, although the precise coordination geometry cannot be conclusively determined from infrared measurements alone. This interpretation agrees with the structural characteristics of dithiocarbamate coordination compounds reviewed by Heard [2]. Similar spectroscopic approaches have been employed in the characterization of metal dithiocarbamate complexes by Abdullah et al. [17]. The consistency of the principal absorption regions across the prepared complexes suggests that the sulfur-containing coordination framework is retained despite the differences in metal identity. Nevertheless, the observed variations in band positions and intensities indicate that coordination environments and electronic interactions may differ among the synthesized compounds.

The nuclear magnetic resonance results provide additional support for the proposed molecular structures of the synthesized complexes. The ^1H NMR spectra of $[PtL_2]$, $[CdL_2]$, and $[HgL_2]$ exhibit NH proton signals at δ 12.34–12.63 ppm, heterocyclic CH signals at δ 6.49–6.62 ppm, and methyl proton signals at δ 3.73–3.83 ppm. These resonances are consistent with the presence of the isoxazole-derived ligand framework in the analyzed compounds. Furthermore, the ^{13}C NMR signals associated with the dithiocarbamate CSS carbon appear at δ 200.26–203.76 ppm, supporting the presence of the sulfur-containing functional group. The phenylmercury complex $[PhHgL]_2$ additionally exhibits aromatic proton resonances around δ 7.37 ppm, consistent with its phenyl substituents. These findings complement the infrared results and strengthen the proposed structural assignments for the diamagnetic complexes examined by NMR spectroscopy. Previous investigations of mercury-containing dithiocarbamate complexes have similarly emphasized the importance of combining spectroscopic techniques to support molecular structural characterization [18]. However, the available NMR measurements do not independently establish the complete coordination geometry or solid-state molecular arrangement, indicating that further structural confirmation would be beneficial.

The powder X-ray diffraction analysis reveals substantial differences in crystallinity among the prepared metal complexes, suggesting that the coordinated metal plays an important role in determining solid-state organization. The $[FeL_2]$ and $[PtL_2]$ complexes exhibit broad diffraction features with relatively weak intensity, consistent with predominantly amorphous structures containing limited short-range order. In contrast, $[CdL_2]$ and $[NiL_2]$ display more pronounced diffraction maxima around $2\theta = 21.5°–22.0°$, together with broad background features characteristic of semi-crystalline materials. The estimated coherent domain sizes of approximately 2.6 nm for $[CdL_2]$ and 2.8 nm for $[NiL_2]$ suggest the presence of nanoscale ordered regions within an amorphous matrix. These findings are relevant to the potential use of dithiocarbamate coordination compounds as precursors or building blocks for functional nanomaterials, as discussed by Sarker and Hogarth [7]. The coexistence of crystalline and amorphous contributions indicates that the synthesized materials possess heterogeneous structural organization rather than uniformly crystalline arrangements. However, the Debye–Scherrer estimates should be

interpreted cautiously because instrumental broadening and contributions from the amorphous phase were not corrected. Consequently, the calculated values provide approximate estimates of coherent diffraction domains rather than direct measurements of individual particle dimensions.

The scanning electron microscopy observations further demonstrate that variations in metal identity are associated with substantial differences in particle morphology and aggregation behavior. The [FeL_2] complex exhibits layered, plate-like, and fibrous structures, whereas [NiL_2] and [CuL_2] display irregular granular particles and extensive agglomeration. The [PtL_2] complex presents fused, irregular aggregates, while [CdL_2] exhibits elongated rod-like and fibrous structures with diameters of approximately 30–80 nm and lengths extending to about 600 nm. In comparison, [HgL_2] forms highly agglomerated, porous, cauliflower-like structures, and [$PhHgL]_2$ displays larger plate-like regions decorated with smaller particles. These morphological differences indicate that metal coordination may influence nucleation, particle growth, aggregation, and the organization of solid materials during synthesis. Comparable investigations of nanoscale metal dithiocarbamate compounds have demonstrated that variations in precursor chemistry can be associated with different structural and morphological characteristics [25]. The SEM observations also complement the XRD results by demonstrating that the prepared materials contain particles and aggregates with dimensions extending beyond those of the estimated coherent crystalline domains. Therefore, the structural differences observed in this study should be understood as the combined outcome of molecular coordination, solid-state organization, and particle aggregation.

Energy-dispersive X-ray spectroscopy provides supporting evidence for the elemental composition of the prepared complexes. The detection of the corresponding metal elements, together with carbon, oxygen, and sulfur, is consistent with the presence of the proposed metal-containing dithiocarbamate materials. Differences in elemental weight percentages among the complexes reflect variations in their elemental composition and the analyzed sample regions. For example, the EDX results show that the [CdL_2] complex contains approximately 38.93 wt.% cadmium, whereas the [PtL_2] complex contains approximately 31.62 wt.% platinum. These results support the incorporation of the corresponding metal elements into the prepared materials and complement the spectroscopic characterization. Nevertheless, EDX is primarily an elemental analytical technique and does not independently confirm molecular bonding configurations, oxidation states, or the proposed stoichiometric formulas. The combined application of FT-IR, NMR, XRD, SEM, and EDX therefore provides a more comprehensive characterization of the synthesized compounds than any individual technique alone. This integrated analytical approach is consistent with previous investigations emphasizing multiple characterization techniques for newly prepared metal dithiocarbamate complexes [24].

The antibacterial evaluation demonstrates that the synthesized complexes possess measurable inhibitory activity against Staphylococcus aureus and Escherichia coli, although their effectiveness varies according to the coordinated metal center. Among the four tested compounds, [PtL_2] exhibits the highest antibacterial activity, producing inhibition zones of 16 mm against S. aureus and 19 mm against E. coli. In contrast, [NiL_2] shows the lowest activity, with inhibition zones of 11 mm and 10 mm against the respective bacterial strains. The [FeL_2] complex produces inhibition zones of 14 mm against S. aureus and 12 mm against E. coli, while [CuL_2] produces values of 13 mm and 14 mm, respectively. These differences suggest that metal identity may influence antibacterial behavior, potentially through changes in molecular interactions, physicochemical properties, or accessibility of the active compound to bacterial cells. Previous studies have reported antibacterial activity among platinum-containing dithiocarbamate complexes, supporting the relevance of this class of coordination compounds for biological investigation [23]. Similarly, investigations of nickel(II)-dithiocarbamate complexes have demonstrated that antibacterial properties can vary with ligand composition and coordination environment [27]. However, the present data do not establish the molecular mechanism underlying the observed inhibition, and additional

experiments would be required to determine whether differences in antibacterial activity arise from metal-dependent biological interactions, compound solubility, diffusion behavior, or other physicochemical factors.

The comparison with tetracycline further clarifies the relative antibacterial performance of the synthesized compounds. Tetracycline produces inhibition zones of 23 mm against S. aureus and 26 mm against E. coli, exceeding the values recorded for all four tested metal complexes. These findings indicate that the synthesized compounds exhibit lower inhibitory activity than the reference antibiotic under the experimental conditions used in this study. The antibacterial ranking against S. aureus follows tetracycline, [PtL_2], [FeL_2], [CuL_2], and [NiL_2], whereas the corresponding ranking against E. coli follows tetracycline, [PtL_2], [CuL_2], [FeL_2], and [NiL_2]. The distinct responses of the two bacterial species suggest that antibacterial effectiveness may depend on both compound characteristics and bacterial cellular properties. The importance of metal coordination in the biological behavior of dithiocarbamate compounds has been discussed in previous studies investigating antimicrobial and cytotoxic properties [19]. Nevertheless, agar diffusion measurements are influenced by compound diffusion, concentration, and solubility, meaning that inhibition-zone diameters should not be interpreted as direct measurements of intrinsic antibacterial potency. Accordingly, minimum inhibitory concentration and minimum bactericidal concentration measurements are needed to confirm and quantitatively compare the antibacterial potential of these complexes.

The combined structural and biological findings suggest a possible relationship between metal coordination characteristics and antibacterial activity, although the available evidence does not establish a direct causal association. The superior inhibitory performance of [PtL_2] compared with [FeL_2], [NiL_2], and [CuL_2] suggests that the platinum-containing coordination environment may be relevant to the observed biological response. However, [PtL_2] exhibits predominantly amorphous XRD characteristics, whereas [NiL_2] contains nanoscale ordered domains, indicating that greater crystallinity does not necessarily correspond to stronger antibacterial activity within this limited series. Likewise, the morphological variation revealed by SEM does not establish a consistent relationship between particle geometry and bacterial inhibition. These observations highlight the importance of distinguishing structural characterization from biological mechanism, particularly when the study involves a limited number of compounds and bacterial strains. The biological activities of isoxazole-containing compounds have been discussed in the medicinal chemistry literature, supporting the selection of the isoxazole scaffold for further investigation [15]. Nevertheless, the present study does not include comparative testing of the free ligand, individual metal salts, or additional control compounds, limiting the ability to isolate the contribution of each structural component. Future investigations incorporating molecular docking, membrane interaction studies, and broader microbiological testing could provide further insight into the mechanisms responsible for the antibacterial behavior.

Overall, the findings contribute to the understanding of isoxazole-functionalized dithiocarbamate complexes by demonstrating that changes in the coordinated metal are accompanied by variations in spectroscopic characteristics, solid-state crystallinity, particle morphology, and antibacterial response. The use of a common ligand framework across the synthesized series provides a basis for comparing the properties of different metal-containing compounds. The results identify [PtL_2] as the most active antibacterial compound among the four complexes tested, while [CdL_2] and [NiL_2] exhibit nanoscale ordered domains within predominantly heterogeneous solid-state structures. These observations establish a preliminary foundation for investigating structure–property relationships in this class of coordination compounds. However, the study is limited by the absence of single-crystal structural determination, quantitative antibacterial susceptibility measurements, cytotoxicity evaluation, and systematic investigation of biological mechanisms. The antibacterial properties of the Cd(II), Hg(II), and phenylmercury(II) derivatives were not evaluated, and their potential toxicological risks would require particular consideration before any biological application. Further studies should therefore integrate advanced structural analysis, minimum inhibitory

concentration testing, mammalian cell toxicity assessment, and mechanistic investigations to determine the suitability of selected complexes for future functional or antimicrobial applications. These additional investigations would help establish whether the observed antibacterial activity can be improved through controlled modification of metal centers, ligand structures, and physicochemical properties.

5. Conclusion

A one-pot route was employed to synthesize and characterize a series of isoxazole derived dithiocarbamate complexes of Fe(II), Ni(II), Cu(II), Pt(II), Cd(II), Hg(II) and phenylmercury(II) by IR, ^{1}H and ^{13}C NMR, XRD, SEM and EDX. Spectroscopic data confirmed bidentate κ 2 -S,S' coordination of the dithiocarbamate ligand. The crystalline character is strongly dependent on the metal ion, as shown by the XRD analysis. The Fe and Pt complexes are essentially amorphous with short-range order, while the Cd and Ni complexes are semicrystalline, with nanosized ordered domains (~2.6–2.8 nm) coexisting with an amorphous phase. SEM images showed different nano-scale morphologies such as plate-like flakes for $[FeL_2]$; granular agglomerates for $[NiL_2]$ and $[CuL_2]$; fused irregular aggregates for $[PtL_2]$; fibrous/rod-like structures for $[CdL_2]$; cauliflower-like porous microstructures for $[HgL_2]$ and bimodal plate-decorated nanostructure for $[PhHgL]_2$. The EDX analysis confirmed the elemental composition and the presence of the expected metal centers. The antibacterial activity of complexes **1**–**4** against Staphylococcus aureus and Escherichia coli demonstrated moderate activity, which was lower than that of the standard drug tetracycline. The order of activity was tetracycline > $[PtL_2]$ > $[FeL_2]$ > $[CuL_2]$ > $[NiL_2]$ against *S. aureus* and tetracycline > [PtL2] > $[CuL_2]$ > $[FeL_2]$ > $[NiL_2]$ against *E. coli*. The platinum complex $[PtL_2]$ was the most active and the nickel complex $[NiL_2]$ was the least active against both strains.

REFERENCES

[1] A. M. Bond and R. L. Martin, "Electrochemistry and redox behaviour of transition metal dithiocarbamates," *Coordination Chemistry Reviews*, vol. 54, pp. 23–98, 1984.

[2] P. J. Heard, "Main group dithiocarbamate complexes," *Progress in Inorganic Chemistry*, vol. 53, pp. 1–69, 2005.

[3] G. Hogarth, "Transition metal dithiocarbamates: 1978–2003," *Progress in Inorganic Chemistry*, vol. 53, pp. 71–561, 2005.

[4] G. Hogarth, "Metal-dithiocarbamate complexes: Chemistry and biological activity," *Mini-Reviews in Medicinal Chemistry*, vol. 12, no. 12, pp. 1202–1215, 2012.

[5] S. Kanchi, P. Singh, and K. Bisetty, "Dithiocarbamates as hazardous remediation agent: A critical review on progress in environmental chemistry for inorganic species studies of 20th century," *Arabian Journal of Chemistry*, vol. 7, no. 1, pp. 11–25, 2014.

[6] A. T. Odularu and P. A. Ajibade, "Dithiocarbamates: Challenges, control, and approaches to excellent yield, characterization, and their biological applications," *Bioinorganic Chemistry and Applications*, vol. 2019, Art. no. 8260496, 2019.

[7] J. C. Sarker and G. Hogarth, "Dithiocarbamate complexes as single source precursors to nanoscale binary, ternary and quaternary metal sulfides," *Chemical Reviews*, vol. 121, no. 10, pp. 6057–6123, 2021.

[8] T. O. Ajiboye, T. T. Ajiboye, R. Marzouki, and D. C. Onwudiwe, "The versatility in the applications of dithiocarbamates," *International Journal of Molecular Sciences*, vol. 23, no. 3, Art. no. 1317, 2022.

[9] N. E. H. Bensiradj, I. N. E. H. Guermi, H. Lemghiti, S. Bessila, L. Boussaid, O. Ouamerali, and A. Zeghdaoui, "Electronic structure and adsorption behaviour of heavy-metal dithiocarbamate complexes on iron oxides: A DFT study toward water remediation," *Molecular Physics*, Art. no. e2692964, 2026.

[10] K. K. Sanjay, "Novel metallomacrocyclic dithiocarbamate complexes and their potential applications in host-guest binding study," Ph.D. dissertation, Maharaja Sayajirao University of Baroda, India, 2023.

[11] T. Saleem *et al*., "Review on the synthesis and potential therapeutic applications of heterocyclic products of 5-amino-3-methylisoxazole," *International Journal of Scientific & Engineering Research*, vol. 12, no. 7, pp. 154–172, 2021.

[12] A. Sysak and B. Obmińska-Mrukowicz, "Isoxazole ring as a useful scaffold in a search for new therapeutic agents," *European Journal of Medicinal Chemistry*, vol. 137, pp. 292–309, 2017.

[13] J. Zhu, J. Mo, H. Z. Lin, Y. Chen, and H. P. Sun, "The recent progress of isoxazole in medicinal chemistry," *Bioorganic & Medicinal Chemistry*, vol. 26, no. 12, pp. 3065–3075, 2018.
[14] C. P. Pandhurnekar, H. C. Pandhurnekar, A. J. Mungole, S. S. Butoliya, and B. G. Yadao, "A review of recent synthetic strategies and biological activities of isoxazole," *Journal of Heterocyclic Chemistry*, vol. 60, no. 4, pp. 537–565, 2023.
[15] G. J. Martis and S. L. Gaonkar, "Advances in isoxazole chemistry and their role in drug discovery," *RSC Advances*, vol. 15, no. 11, pp. 8213–8243, 2025.
[16] A. S. Al-Janabi, M. M. Kadhim, A. I. Al-Nassiry, and T. A. Yousef, "Antimicrobial, computational, and molecular docking studies of Zn(II) and Pd(II) complexes derived from piperidine dithiocarbamate," *Applied Organometallic Chemistry*, vol. 35, no. 2, Art. no. e6108, 2021.
[17] T. B. Abdullah *et al.*, "Cd(II) and Pd(II) mixed ligand complexes of dithiocarbamate and tertiary phosphine ligands—spectroscopic, anti-microbial, and computational studies," *Molecules*, vol. 28, no. 5, Art. no. 2305, 2023.
[18] A. I. Al-Nassiry, A. S. Al-Janabi, O. Y. Thayee Al-Janabi, P. Spearman, and M. A. Alheety, "Novel dithiocarbamate–Hg(II) complexes containing mixed ligands: Synthesis, spectroscopic characterization, and H2 storage capacity," *Journal of the Chinese Chemical Society*, vol. 67, no. 5, pp. 775–781, 2020.
[19] A. S. Al-Janabi, A. M. Saleh, and M. R. Hatshan, "Cytotoxicity, anti-microbial studies of M(II)-dithiocarbamate complexes, and molecular docking study against SARS COV2 RNA-dependent RNA polymerase," *Journal of the Chinese Chemical Society*, vol. 68, no. 6, pp. 1104–1115, 2021.
[20] S. A. Al-Jibori, A. S. Al-Janabi, S. W. Al-Sahan, and C. Wagner, "Pd(II)-pyrrolidine dithiocarbamate complexes: Synthesis, spectroscopic studies and molecular structure of [Pd(PyDT)(ppy)]," *Journal of Molecular Structure*, vol. 1227, Art. no. 129524, 2021.
[21] T. B. Abdullah, H. M. Jirjes, A. S. Faihan, and A. S. Al-Janabi, "Spectroscopic, computational, anti-bacterial studies of bivalent metal complexes of N-picolyl-amine dithiocarbamate," *Journal of Molecular Structure*, vol. 1276, Art. no. 134730, 2023.
[22] E. M. Al-Janabi, M. A. Alheety, S. A. Al-Jibori, A. S. Faihan, and A. S. Al-Janabi, "Hydrogen adsorption of some new mercury(II)-benzotriazole dithiocarbamate mixed ligand complexes: Kinetic studies," *Journal of the Iranian Chemical Society*, vol. 20, no. 8, pp. 1781–1790, 2023.
[23] E. M. Al-Janabi, M. R. Hatshan, S. F. Adil, W. R. Kadhum, S. A. Al-Jibori, A. S. Faihan, and A. S. Al-Janabi, "Spectroscopic, antibacterial and anti-cancer studies of new platinum(II)-diethyldithiocarbamate mixed ligand complexes with phosphine or amine ligands," *Journal of Molecular Structure*, vol. 1252, Art. no. 132227, 2022.
[24] I. F. Alshdoukhi, A. S. Al-Barwari, N. M. Aziz, T. Khalil, A. S. Faihan, S. A. Al-Jibori, and A. S. Al-Janabi, "Pd(II), Pt(II), Zn(II), Cd(II) and Hg(II) complexes of the newly prepared 1,2-benzoisothiazol-3(2H)-dithiocarbamate (BIT-DTC) ligand," *Bulletin of the Chemical Society of Ethiopia*, vol. 38, no. 4, p. 889, 2024.
[25] M. M. Salman, A. A. Al-Dulaimi, A. S. Al-Janabi, and M. A. Alheety, "Novel dithiocarbamate nano Zn(II), Cd(II) and Hg(II) complexes with pyrrolidinedithiocarbamate and N,N-diethyldithiocarbamate," *Materials Today: Proceedings*, vol. 43, pp. 863–868, 2021.
[26] M. M. Kadhim, L. A. A. Juber, and A. S. Al-Janabi, "Estimation of the efficiency of corrosion inhibition by Zn-dithiocarbamate complexes: A theoretical study," *Iraqi Journal of Science*, pp. 3323–3335, 2021.
[27] T. A. Yousef, A. S. Al-Janabi, S. Shaaban, and O. K. Al-Duaij, "Nickel(II)-dithiocarbamate mixed ligand complexes: Synthesis, characterization and anti-bacterial properties," *Oriental Journal of Chemistry*, vol. 41, no. 2, 2025.
[28] A. S. Al-Janabi *et al.*, "Phenyl mercury(II)-pyrrolidinedithiocarbamate complexes: Spectroscopic studies, along with Hirshfeld surface, DFT studies and crystal structure of [PhHg(κ3N,S,S-PyDT)]2," *Journal of Molecular Structure*, Art. no. 143342, 2025.
[29] J. O. Adeyemi and D. C. Onwudiwe, "Organotin(IV) dithiocarbamate complexes: Chemistry and biological activity," *Molecules*, vol. 23, no. 10, Art. no. 2571, 2018.
[30] Y. S. Tan, C. I. Yeo, E. R. T. Tiekink, and P. J. Heard, "Dithiocarbamate complexes of platinum group metals: Structural aspects and applications," *Inorganics*, vol. 9, no. 8, Art. no. 60, 2021.
[31] N. Manav, A. K. Mishra, and N. K. Kaushik, "In vitro antitumour and antibacterial studies of some Pt(IV) dithiocarbamate complexes," *Spectrochimica Acta Part A: Molecular and Biomolecular Spectroscopy*, vol. 65, no. 1, pp. 32–35, 2006.
[32] D. J. Berry, R. Torres Martin de Rosales, P. Charoenphun, and P. J. Blower, "Dithiocarbamate complexes as radiopharmaceuticals for medical imaging," *Mini-Reviews in Medicinal Chemistry*, vol. 12, no. 12, pp. 1174–1183, 2012.

[33] M. D. Regulacio *et al*., "Luminescence of Ln(III) dithiocarbamate complexes (Ln = La, Pr, Sm, Eu, Gd, Tb, Dy)," *Inorganic Chemistry*, vol. 47, no. 5, pp. 1512–1523, 2008.
[34] V. A. Fitsanakis, V. Amarnath, J. T. Moore, K. S. Montine, J. Zhang, and T. J. Montine, "Catalysis of catechol oxidation by metal-dithiocarbamate complexes in pesticides," *Free Radical Biology and Medicine*, vol. 33, no. 12, pp. 1714–1723, 2002.